ACS OMEGA

http://pubs.acs.org/journal/acsodf

Article

Visible-Light-Driven Photocatalytic Degradation of Tetracycline Using Heterostructured Cu_2O–TiO_2 Nanotubes, Kinetics, and Toxicity Evaluation of Degraded Products on Cell Lines

Manisha Sharma, Mrinal Kanti Mandal, Shailesh Pandey, Ravi Kumar, and Kashyap Kumar Dubey*

Cite This: *ACS Omega* 2022, 7, 33572–33586

Read Online

ACCESS | Metrics & More | Article Recommendations | Supporting Information

ABSTRACT: This study first reports on the tetracycline photodegradation with the synthesized heterostructured titanium oxide nanotubes coupled with cuprous oxide photocatalyst. The large surface area and more active sites on TiO_2 nanotubes with a reduced band gap (coupling of Cu_2O) provide faster photodegradation of tetracycline under visible light conditions. Cytotoxicity experiments performed on the RAW 264.7 (mouse macrophage) and THP-1 (human monocytes) cell lines of tetracycline and the photodegraded products of tetracycline as well as quenching experiments were also performed. The effects of different parameters like pH, photocatalyst loading concentration, cuprous oxide concentration, and tetracycline load on the photodegradation rate were investigated. With an enhanced surface area of nanotubes and a reduced band gap of 2.58 eV, 1.5 g/L concentration of 10% C-TAC showed the highest efficiency of visible-light-driven photodegradation (~100% photodegradation rate in 60 min) of tetracycline at pH 5, 7, and 9. The photodegradation efficiency is not depleted up to five consecutive batch cycles. Quenching experiments confirmed that superoxide radicals and hydroxyl radicals are the most involved reactive species in the photodegradation of tetracycline, while valance band electrons are the least involved reactive species. The cytotoxicity percentage of tetracycline and its degraded products on RAW 264.7 (−0.932) as well as THP-1 (-0.931) showed a negative correlation with the degradation percentage with a *p*-value of 0.01. The toxicity-free effluent of photodegradation suggests the application of the synthesized photocatalyst in wastewater treatment.

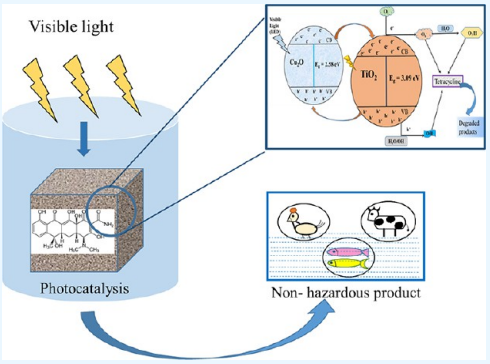

1. INTRODUCTION

Tetracyclines (TCs) are the most used antibiotics after sulfonamides in the human health care and animal husbandry sector because of their broad-spectrum antimicrobial activity.[1−4] In 2020, ECDC (European Center for Disease Prevention and Control) reported that out of the total consumed anti-infectives per day [32.62 DDD (defined daily doses) per 1000 inhabitants], 9.21% were TCs (3.00 DDD per 1000 inhabitants) (https://www.ecdc.europa.eu/en/antimicrobial-consumption/database/rates-country). Because of the poor metabolic degradation rate, 95% of TC was excreted out and finally reached the aquatic environment through the sewage system,[5−7] and thus, the presence (ng/L to mg/L) is common in the aquatic environment.[8−13]

TC in the native form and its metabolites have hydrophilicity, biological activity, and stability, which is highly toxic to the non-target aquatic organisms.[14,15] The slow degradation rate and high persistence of antibiotics in the environment result in the development of antimicrobial resistance in microorganisms reported against TC, followed by sulfonamides.[16−18] Accumulation and transmission of antibiotics through the food chain in the environment cause serious threats to human beings and the ecosystem due to the vertical and horizontal transfer of antibiotic-resistant genes. This may lead to the disappearance of some species, causing ecological imbalance.[19,20]

Several degradation and removal of antibiotic treatment technologies are developed, such as biological, chemical, and physical and the combination thereof from the aquatic ecosystem. Biological degradation of antibiotics with fungi and biocatalysts is reported in many studies, but it is not the method of choice for degradation of antibiotics because of a low biodegradation rate and the non-biodegradable nature of antibiotics.[21−23] Low efficiencies of degradation methods of membrane-based (ultra- and nanofiltrations) physical treatments make them not suitable for the degradation of antibiotics. Chemical methods include photo-Fenton, ozonation, photolysis, and semiconductor-based photocatalysis explored for the degradation and removal of antibiotics, but every method had its limitations. For example, secondary pollution, use of harmful

Received: July 20, 2022
Accepted: September 1, 2022
Published: September 9, 2022

chemicals, and high-cost inputs were the limitations of ozonation and Fenton-based degradation and the electrochemical oxidation method of degradation.[24−31]

Advanced oxidation processes (AOPs) are one of the extensively used methodologies for the treatment of wastewater/effluents which utilize highly reactive and oxidizing species (O_3, $^{\bullet}O_2$, H_2O_2, $OH^{\bullet}$) for the complete degradation of the target compounds into carbon dioxide and water.[32] Photocatalysis is the most studied and promising AOP technology used for the degradation of antibiotics as there is no requirement of any additional chemicals and it can be performed under light and pressure conditions under a mild temperature.[33−36] Environment-friendly implementation of photocatalytic approaches enables the use of a highly efficient technique for the degradation of antibacterial compounds with complete mineralization.[37] TiO_2 is the most studied and used photocatalyst for the removal of antibiotics from wastewater. However, the large band gap limits the photoabsorbance in visible light and is a hindrance to the exploitation of the energetic potential for degradation and removal of antibiotics from wastewater.[38,39] The efficiency of the semiconductor-based photocatalyst was enhanced with doping, heterogeneous composition, noble metal deposition, use of supportive materials, use of hybrid nanomaterials, and surface modification of the photocatalyst by using an alternative method of synthesis.[37,40−50]

Studies reported that coupling of p-type TiO_2 with the n-type of metal oxide semiconductors like Cu_2O is an effective way to decrease the band gap with enhanced photocatalytic activity of the heterojunction p−n-type photocatalyst.[51,52] Being a photoactive transition metal, doping of copper in a semiconductor photocatalyst modifies the electronic and photophysical properties of the photocatalyst. Copper 3d orbital electrons changed the valance band in the dopant state, which further broaden the adsorption range to the visible light. The reduced band gap in the cuprous oxide-doped TiO_2-based photocatalyst enhances the photodegradation efficiency of the system.[53] Cu_2O-doped TiO_2 nanotubes have more efficient visible-light-drawn photocatalytic activity than TiO_2, which further enhances the light harvesting in a longer wavelength and more effective transfer of photogenerated carriers. Moreover, the presence of cuprous oxide enhances the adsorption efficiency, and thus, more exposure of functional groups of antibiotics on the heterogeneous photocatalyst leads to increased photodegradation.[54]

The present study focused on the photocatalytic degradation of TC using synthesized titanium oxide nanotubes coupled with cuprous oxide nanoparticles. Photocatalyst load, antibiotic concentration, pH, and cuprous oxide loading concentration were used as variable parameters to maximize the photodegradation of TC. The role of cuprous oxide doping for enhanced photodegradation of TC was investigated, and the optimal cuprous oxide loading concentration for a high degradation efficiency was identified. The toxicity of parent and degraded compounds was examined against mammalian cell lines. Toxicity percentages were correlated with the degradation percentages to confirm the loss of biological activity of TC via photodegradation. Quenching experiments and mass spectrometric studies were used to propose the mechanism of photodegradation of TC.

The novelty of the present study provides environment-friendly photodegradation of TC with the synthesized Cu_2O−TiO_2 nanotubes and thus avoids its leakage into the environment with non-hazardous products in the effluent water. TiO_2 nanotubes provide more surface area and active sites of photodegradation than TiO_2 nanoparticles, while the coupling of Cu_2O reduces the band gap so that short-wavelength radiations (visible light) can be used as photon energy for photodegradation of TC. Visible-light-based photodegradation allowed the use of renewable energy (solar light) as a cost-effective wastewater treatment process with the aim of faster photodegradation and reusability of the photocatalyst. Also, the transformed and degraded products have not shown any cytotoxicity in the final effluent of the treatment process. Thus, the developed photocatalyst fulfils all the criteria (a high photocatalytic efficiency, full use of solar light, and high recyclability) required for the industrialization of photocatalysis with toxicity-free effluent water as the most promising treatment process for the antibiotic-containing wastewater.

2. MATERIALS AND METHODS

2.1. Chemicals and Reagents. For TiO_2 nanotube preparation, titanium(IV) oxide was used as a precursor and was purchased from Merck Life Sciences Pvt. Ltd. (India). Sodium hydroxide (NaOH), hydrochloric acid (HCl), and TC hydrochloride were purchased from BR Biochem Life Sciences Pvt. Ltd. (India). Ultra-pure water was prepared with a Milli-Q water purification system (ELGA-PURELAB Pulse, UK). High-performance liquid chromatography (HPLC) grade acetonitrile, water, formic acid, and methanol were purchased from Thermo Fisher Scientific India Pvt. Ltd. (India). Sodium azide, sodium nitrate, ammonium oxalate, and *p*-benzoquinone were purchased from Merck Life Sciences Pvt. Ltd. (India). All the solvents and reagents were of analytical grade, and Milli-Q water was used for the preparation of solutions.

2.2. Preparation of Cu_2O-Doped TNT Particles. *2.2.1. Synthesis of TiO_2 Nanotubes.* TiO_2 nanotubes (TNTs) were synthesized using the same procedure as that described in ref 55 and with some modifications in the procedure, and these particles were named TAC (TNT-applied catalysis). 1.0 g of TiO_2 nanoparticles (titanium(IV) oxide) was dispersed into 30 mL of 10 M sodium hydroxide solution. The suspension was stirred vigorously for 2 h at 30 °C. Then, the suspension was autoclaved at 140 °C for 24 h. The product obtained was redispersed in 200 mL of a 0.1 M HCl solution for 3 h. Then, the suspension was centrifuged and the solid sample was washed with distilled water until the pH was stabilized at 6.7. Finally, the sample was dried at 80 °C for 24 h in a vacuum oven. The dried sample was then annealed at 350 °C for 6 h.

2.2.2. Cuprous Oxide Doping. First, copper sulfate pentahydrate was dispersed into 70 mL of water. Then, 2 g of TNT/TAC and 2.4 g (1 M aq) of NaOH were added to the solution and stirred for 1 h. Dextrose (2 g) was then added to the green suspension during stirring. The resulting suspension was then transferred into a 100 mL Teflon container and cooked in a hydrothermal vessel at 150 °C for 12 h. Finally, the product was collected and washed with distilled water and ethanol several times. In the end, products were dried in a hot air oven at 60 °C for 12 h to gain Cu_2O-TAC/TNT. Cu_2O-TAC with different weight percentages of Cu_2O (5, 10, and 20) was labeled as 5% C-TAC, 10% C-TAC, and 20% C-TAC.

Chemical reaction

https://doi.org/10.1021/acsomega.2c04576
ACS Omega 2022, 7, 33572−33586

$$\underset{\text{Copper Sulphate}}{2CuSO_4} + 4NaOH \rightarrow \underset{\text{Cuprous oxide}}{Cu_2O} + 2Na_2SO_4 + 2H_2O + 1/2O_2$$

2.3. Characterization of the Photocatalyst. The crystal structure of the prepared photocatalyst was determined by X-ray diffraction (XRD), while the morphology was observed via scanning electron microscopy (SEM). Ultraviolet−visible−near-infrared (UV−vis−NIR) spectroscopy was used for the determination of the light-harvesting capabilities of the synthesized photocatalysts via absorption and transmittance spectra. The absorbance and transmittance data were then used to calculate the band gap energy of all the developed photocatalysts according to the Kubelka−Munk equation.[56] The photocatalytic activity of a photocatalyst is dependent on band gap energy; the lower the band gap, the higher will be the photocatalytic efficiency of the photoreactor.[57]

2.4. Photoreactor System Design. A photochemical apparatus was designed for the degradation of TC from aquatic solutions. The photodegradation was carried out in a quartz flask reactor system. The reactor was placed in a laboratory-constructed wooden box with a glass mirror attached to the inner wall to maximize the light absorption. The box was equipped with UV light (5 × 11 W of each) and LED visible light (2 × 50 W of each) and arranged in such a way that the distance of the light source to the reactor vessel was not greater than 15 cm. The reaction was carried out on the hot plate magnetic stirrer fitted inside the box for the continuous stirring of solutions. An exhaust fan was positioned on the back side of the box to obviate the heating effect of light. The effects of selected parameters (photocatalyst load, antibiotic concentration, pH condition, cuprous oxide loading concentration) on the removal efficiency of the photocatalytic system were evaluated. The schematic diagram of the photocatalytic setup is shown in Figure S1.

2.5. Photodegradation Study. The photocatalytic experiments were carried out to evaluate the effect of different parameters and to identify the optimized parameters for the efficient degradation of TC. The effect of all selected parameters was evaluated in the photoreactor system with ambient temperature and pressure conditions. The reaction mixture was stirred in the dark for 30 min to achieve adsorption of TC and the TiO_2-based photocatalyst. Light irradiation (UV and/or visible) was used for photodegradation of TC, and periodically after every 30 min, 3 mL of the sample was drawn from the photoreactor vessel. Further, 2 mL of the sample was centrifuged, followed by filtration by 0.2 μm syringe filters before HPLC analysis, while 1 mL of the sample was stored for further toxicity analysis. The concentration of TC was identified from the characteristics of the absorbance area of HPLC at 354 nm. The degradation efficiency was calculated using eq 1

$$\text{Degradation } \% = \frac{C_o - C_t}{C_o} \times 100 \quad (1)$$

where C_o is the concentration of TC at the beginning of experiments and C_t is the concentration of TC in the sample collected after time t.

LC−MS analysis was used to confirm the degradation of TC and to identify the intermediate products of TC photodegradation. Further, quenching experiments were done to determine the role of different reactive oxygen species in the photocatalytic degradation of TC. Formic acid/ammonium oxalate, methanol/*tert*-butanol, *p*-benzoquinone, sodium azide, and silver nitrates/potassium dichromate were used as hole (h_{VB}^+) scavengers, hydroxyl radical ($HO^\bullet$) scavengers, superoxide radical ($O_2^{\bullet-}$) scavengers, singlet oxygen (O_2) scavengers, and electron (e_{CB}^-) scavengers, respectively. 20 mM concentration of the scavenger was used with all the other control conditions (optimized conditions of the selected photocatalyst) to confirm their role in photodegradation of TC.

2.6. Analytical Method. The concentration of TC was measured using a CECIL HPLC system with a UV−vis detector (CE4200) at a wavelength of 354 nm. TC (HCl) (BR Biochem-BC0504) was used to develop a standard curve for the estimation of TC amount in photodegraded samples. 1000 μg/mL stock solution was prepared in water, and different dilutions were done (750, 500, 250, 100, 50, 10, 1 μg/mL). The mobile phase, the ratio of the mobile phase, the gradient/static run, the column temperature, and the flow rate were standardized for the detection of TC,[58] and the analysis was performed at 354 nm with water (0.01% formic acid) and acetonitrile (0.01% formic acid) as the mobile phase with a flow rate of 1.0 mL/min and 20 °C column temperature in a gradient run of 17 min. Mass spectrometry of native and degraded samples was done using a Q Exactive Plus Hybrid Quadrupole-Orbitrap Mass Spectrometer (Thermo-Fisher).

2.7. Kinetics Study of Photodegradation Reaction. The rate of photodegradation of TC was studied with the Langmuir−Hinshelwood model, and a linear reciprocal relation was observed between the rate of degradation and the concentration of TC (substrate) in the reaction solution

$$r = -\frac{\text{d[concentration of tetracycline]}}{dt} = KC$$

$$\ln C_t = \ln C_o - kt$$

$$\ln\left(\frac{C_t}{C_o}\right) = -kt$$

where C_t is the concentration of TC in the sample collected after time t, C_o is the initial concentration of TC, and k is the rate constant of the photodegradation reaction.

2.8. Toxicity Analysis. The toxicity of TC and its degraded compounds were checked on the mouse macrophage (RAW 264.7) and human monocyte (THP-1) cell lines after 48 h. The cell lines were grown on the specified medium [Dulbecco's modified Eagle's medium for RAW 246.7 and Roswell Park Memorial Institute (RPMI) −1640 for THP-1 cell lines] and under suitable environmental culture conditions (37 °C + 5% CO_2). The sufficiently grown cells (1 × 10^4 cells/mL) were further seeded to 96-well plates for toxicity assay. MTT (3-(4,5-dimethylthiazol-2-yl)-2,5-diphenyltetrazolium bromide) reduction assay was performed to examine the viability of cells as a toxicity testing endpoint. Figure S2 shows the brief methodology followed[59] during the cytotoxicity testing of parent as well as transformed antibiotics. The viability of cells was determined calorimetrically at 570 nm. The toxicity of compounds was determined by eq 2

$$\text{Cytotoxicity } \% = 100 - \left(\frac{\text{Absorbance(Sample)}}{\text{Absorbance(Control)}}\right) \times 100 \quad (2)$$

https://doi.org/10.1021/acsomega.2c04576
ACS Omega 2022, 7, 33572−33586

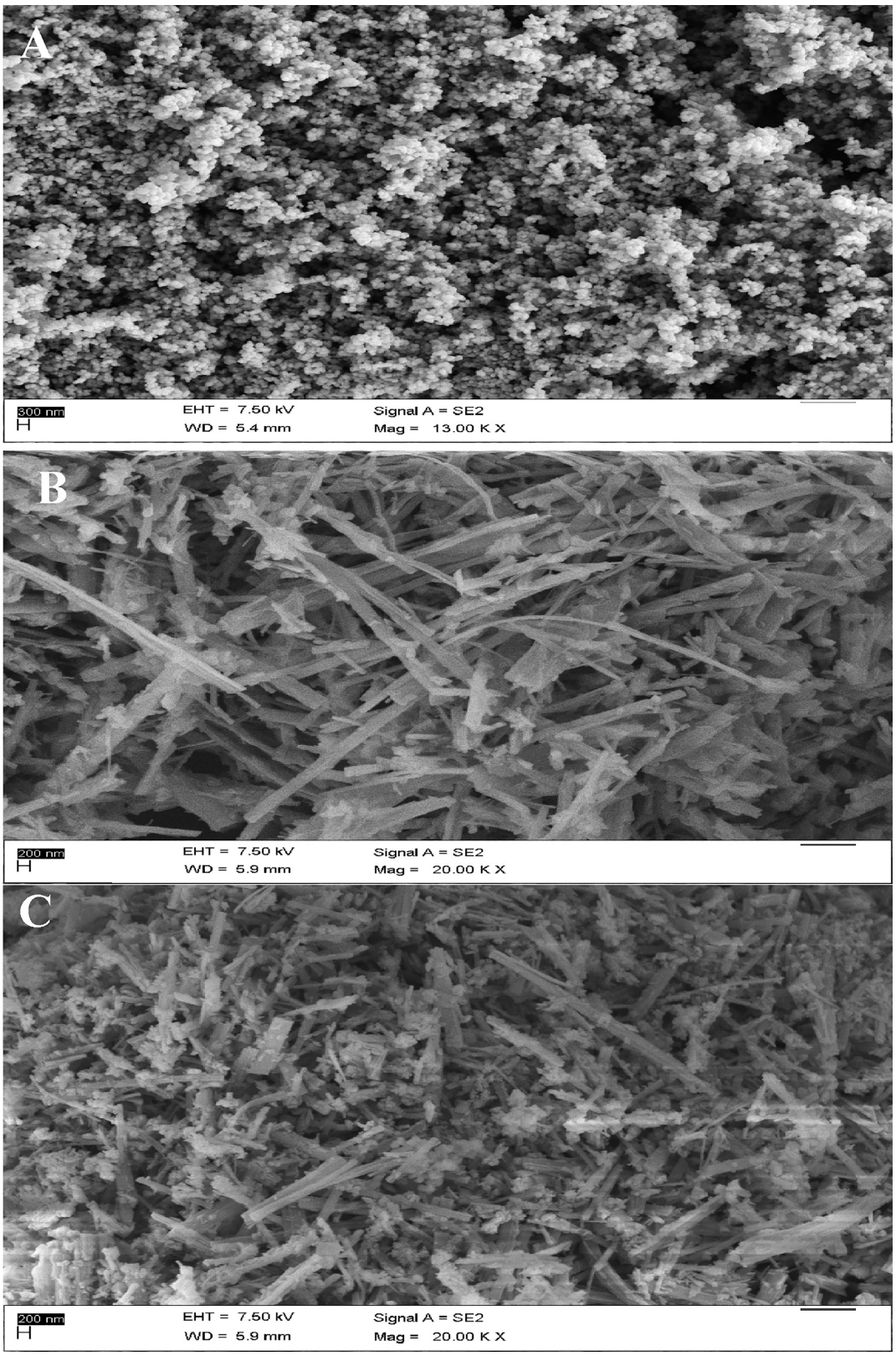

Figure 1. SEM image (A) of titanium (IV) oxide, (B) titanium oxide nanotubes, and (C) 10% Cu_2O-TiO_2 nanotubes.

3. RESULTS AND DISCUSSION

3.1. Photocatalyst Characterization. SEM images of prepared photocatalysts were analyzed to examine the microstructure and topology of all the synthesized samples. Figure 1A unveils the asymmetrical granular morphology of the raw titanium(IV) oxide nanoparticles, used to synthesize TiO_2 nanotubes. These particles are in nearly a round shape having the least surface area. An ideal photocatalyst should have a bigger surface area to provide more interactive sites to target compounds, resulting in improved photocatalysis reaction.

https://doi.org/10.1021/acsomega.2c04576
ACS Omega 2022, 7, 33572−33586

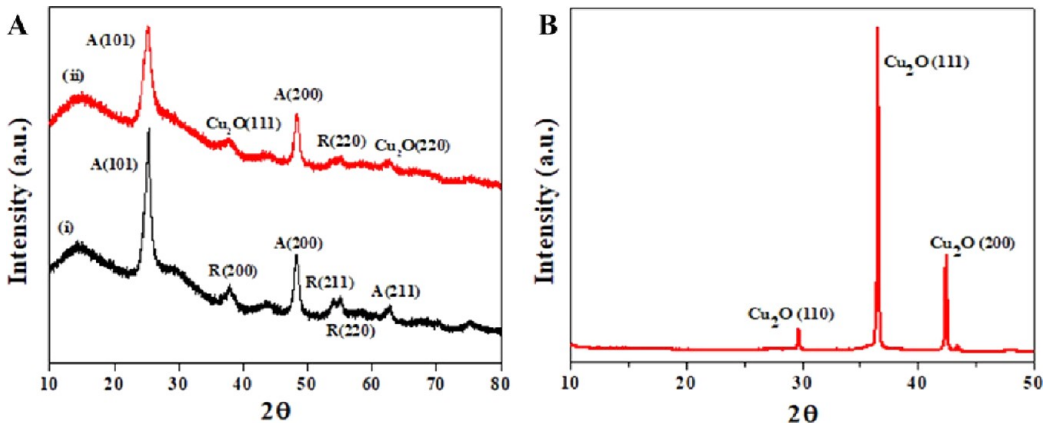

Figure 2. (A) XRD diffractograms of synthesized photocatalysts (TAC) and 10% Cu_2O-TiO_2 nanotubes (C-TAC); (B) XRD diffractogram of Cu_2O reduced from $CuSO_4 \cdot 5H_2O$.

Thus, TiO_2 nanoparticles were modified to TiO_2 nanotubes which own a greater surface area (Figure 1B). A lengthened tubular morphology was displayed by the modified TiO_2 sample which promulgated the reduced aggregation of nanotubes as a consequence of alkaline hydrothermal operation and calcination. SEM images suggested that the prepared nanotubes have an enhanced surface area, and also, there is a higher surface area to volume ratio. This result is consistent with the previous study reported by Zavala et al.[60] Figure 1C demonstrates the grafting of 10% Cu_2O nanoparticles (small granular particles) over TNT/TAC nanotubes known as C-TAC. Cu_2O and TNT form a coupled semiconductor making the whole heterostructured photocatalyst workable even in visible light. XRD analysis was performed to determine the crystal structure and phase orientation of the used photocatalysts and 10% Cu_2O-TiO_2 nanotubes. The diffractogram shown in Figure 2A plot (i) clarifies the presence of crystalline anatase phase A (101) at 25.349°, A (200) at 48.23°, and A (211) at 55.160° in synthesized TiO_2 nanotubes. A trace amount of the rutile phase (R) of TiO_2 was also observed at 37.811, 53.934, and 55.160° in the shape of 200, 211, and 220 packings, respectively. Sharp peaks of the diffractogram confirmed the strong crystalline anatase phase of TiO_2 in the synthesized photocatalyst. Diffraction due to Cu_2O appeared at the 38.0037 and 62.7788° in the shape of 111 and 220 packings, respectively (Figure 2A plot (ii)). These peaks and SEM images of Cu_2O/TiO_2 nanotubes confirmed the coupling of Cu_2O on the modified TiO_2 nanotubes. In this plot, the intensities of the anatase phase were reduced with increased peak width at the baseline. These changes in diffractograms may be attributed due to the effect of Cu_2O coupling with TiO_2 nanotubes. The strong crystalline phase of Cu_2O appeared at 29.73, 36.578, and 42.469° with crystalline packings of 110, 111, and 200, respectively (Figure 2B). This result again confirmed the formation of cuprous oxide in the developed visible-light-active photocatalyst.

The Fourier-transform infrared spectroscopy (FT-IR) spectra of TiO_2 nanotubes and 10% Cu_2O/TiO_2 nanotube samples were recorded in the wavenumber range of 400−4000 cm^{-1}. Figure 3 shows the bonding interactions present in all the synthesized samples. Broadbands were observed between 3300 and 3450 cm^{-1}, corresponding to the O−H bond's stretching vibrations in both the samples, as mentioned earlier. The bending vibration of the O−H bond was observed between 1500 and 1700 cm^{-1}.[61] The bands between 600 and 900 cm^{-1}

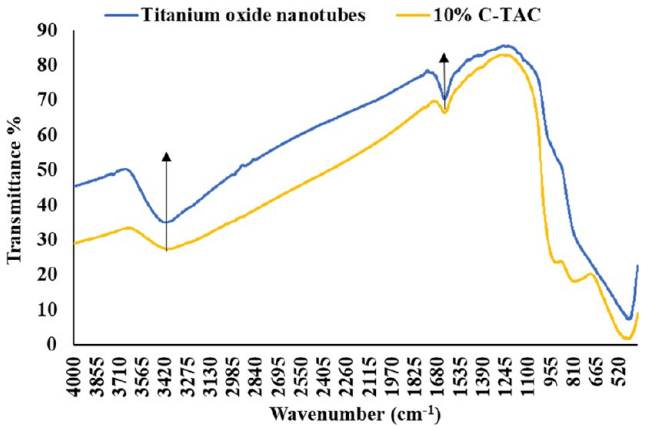

Figure 3. FT-IR spectrum of the synthesized photocatalyst.

represent Ti−O−Ti vibration signals.[62] The spectrum shows similar trends in both the samples and describes the well-built interactions between Cu_2O nanoparticles and TNTs.[63] Another noteworthy inspection is the shift in the absorbance intensity of bands between 3400−3500 and 700−800 cm^{-1} to the lower wavenumbers in the case of the sample incorporated with Cu_2O. These bands specify the successful deposition of Cu_2O nanoparticles on the lattice of the host TiO_2.[64]

The results, obtained from the XPS (X-ray photon spectroscopy) characterization of 10% Cu_2O/TiO_2 nanotubes shown in Figure 4A, were used to investigate the elemental composition, surface defects, and chemical environment of the prepared photocatalyst. The dominant peaks in the XPS result are the Cu, Ti, and O peaks, suggesting a successful formation of the heterostructure composite photocatalyst. There is a peak related to carbon at 288.62 eV. This appearance might be related to hydrocarbon contamination in the apparatus during the characterization. The peaks located at 932.1 and 952.0 eV in Figure 4B can be ascribed to those of Cu $3d_{3/2}$ and Cu $3d_{1/2}$ from Cu_2O, respectively. In the same way, Figure 4C represents the deconvoluted peaks for TiO_2 associated to Ti $2p_{3/2}$ and Ti $2p_{1/2}$ at 458 and 463.81 eV, respectively. Figure 4 A shows that the binding energy of O 1s is 531.6 eV, which is consistent with the O 1s of O^{2-}. Therefore, the XPS spectra confirm that the Cu_2O/TiO_2 nanocomposite is essentially composed of Ti^{2+}, Cu^{2+}, and O^{2-}.

From the UV−vis−NIR absorbance data, the band gap was calculated for each modified photocatalyst according to the

https://doi.org/10.1021/acsomega.2c04576
ACS Omega 2022, 7, 33572−33586

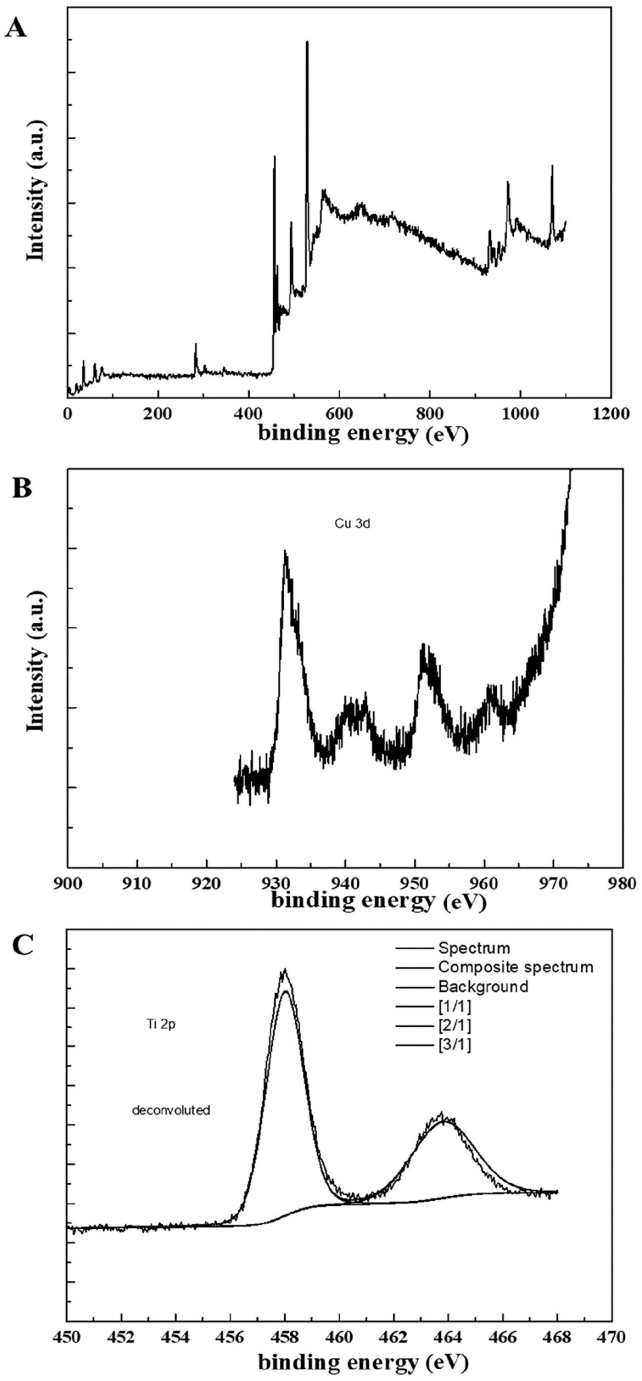

Figure 4. (A) XPS analysis of the photocatalyst 10% Cu_2O/TiO_2 nanotubes; (B) Cu 3d narrow scan spectrum; (C) Ti 2p narrow scan spectrum.

Kubelka–Munk model and it was found that the band gap was shortened up to 2.58 eV (10% cuprous oxide doping) (Table 1). Doping of cuprous oxide effectively shifts the absorbance from NIR (400 nm) to the visible light range (479 nm) (Figure 5). Similar results of reduction of band gap energy with copper doping ($Cu-TiO_2$) were reported by other researchers.[65,66]

3.2. Effect of Different Parameters on Photodegradation Rate. *3.2.1. Photocatalyst Loading Effect.* Photocatalyst concentration directly affects the degradation efficiency. In general, the degradation efficiency of TC increased with increased concentration of the photocatalyst. Figure 6A shows

Table 1. Band Gap Energy of the Developed Photocatalyst

photocatalyst	cut-off wavelength (nm)	band gap (eV)	R^2
TNT	400.51	3.10	0.9708
TAC	401.25	3.09	0.9885
5% C-TAC	447.20	2.77	0.9952
	nanotubes		
20% C-TAC	440.49	2.81	0.9954
10% C-TAC	479.57	2.58	0.9969
10% C-TNT	473.83	2.63	0.9918

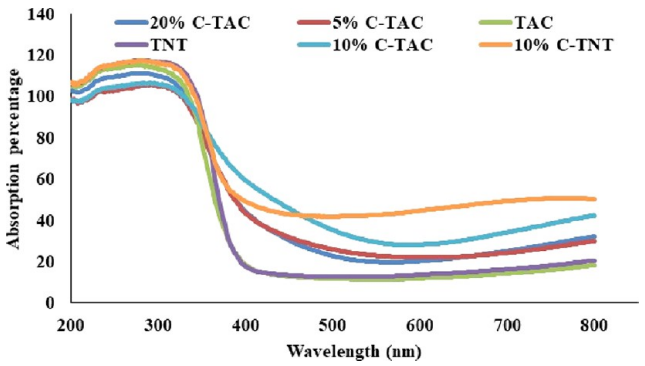

Figure 5. UV–vis DRS spectrum of all the synthesized photocatalysts.

the degradation rate of TC with different concentrations of TNT and TAC. Without the photocatalyst, negligible degradation was observed, but after the addition of the photocatalyst, the degradation rate was enhanced. The optimum concentration of the photocatalyst showing maximum degradation was 1.5 g/L in both TNT and TAC. Both the photocatalysts were TiO_2-based photocatalysts and differ only in the method of preparation. Thus, there was not so much difference in degradation efficiency. This result was consistent with DRS results. Beyond this (1.5 g/L), the enhancement in degradation efficiency was not observed with increased photocatalyst concentration. The reason behind this could be the high viscosity of the solution, blockage in penetration of light, sedimentation, and elimination of effective sites of photodegradation. The same concentration of titania P-25 degussa (1.5 g/L) was used by Palominos (2009) and co-workers for photocatalytic degradation of TC,[67] whereas Reyes and co-workers found that 0.5 g/L concentration of titania P-25 degussa (TiO_2) is optimum to degrade TC.[68] Similarly, Safari and co-workers estimated 1.0 g/L as the optimum concentration of nanosized titanium dioxide for photocatalytic degradation of TC.[69]

3.2.2. Antibiotic Concentration Effect. A variable range of initial concentrations of the antibiotic (50–1000 ppm) was evaluated for their effect on degradation efficiency. Figure 6B shows that the photodegradation percentage of TC was decreased with the increased initial concentration of the antibiotic. Identical results were shown by the report of other researchers.[69,70] Similar trends of effects of initial concentration of TC on photodegradation were observed with TiO_2 sulfur-doped carbon nitride nanocomposites.[71] During the initial hour of photodegradation experiments, the degradation percentage with an initial concentration of 100 ppm was better than that with the initial concentration of 50 ppm. However, at the end of the experiments, the degradation rate with 50 ppm concentration overcomes the degradation rate with 100 ppm. The increased initial concentration of TC resulted in less availability

https://doi.org/10.1021/acsomega.2c04576
ACS Omega 2022, 7, 33572–33586

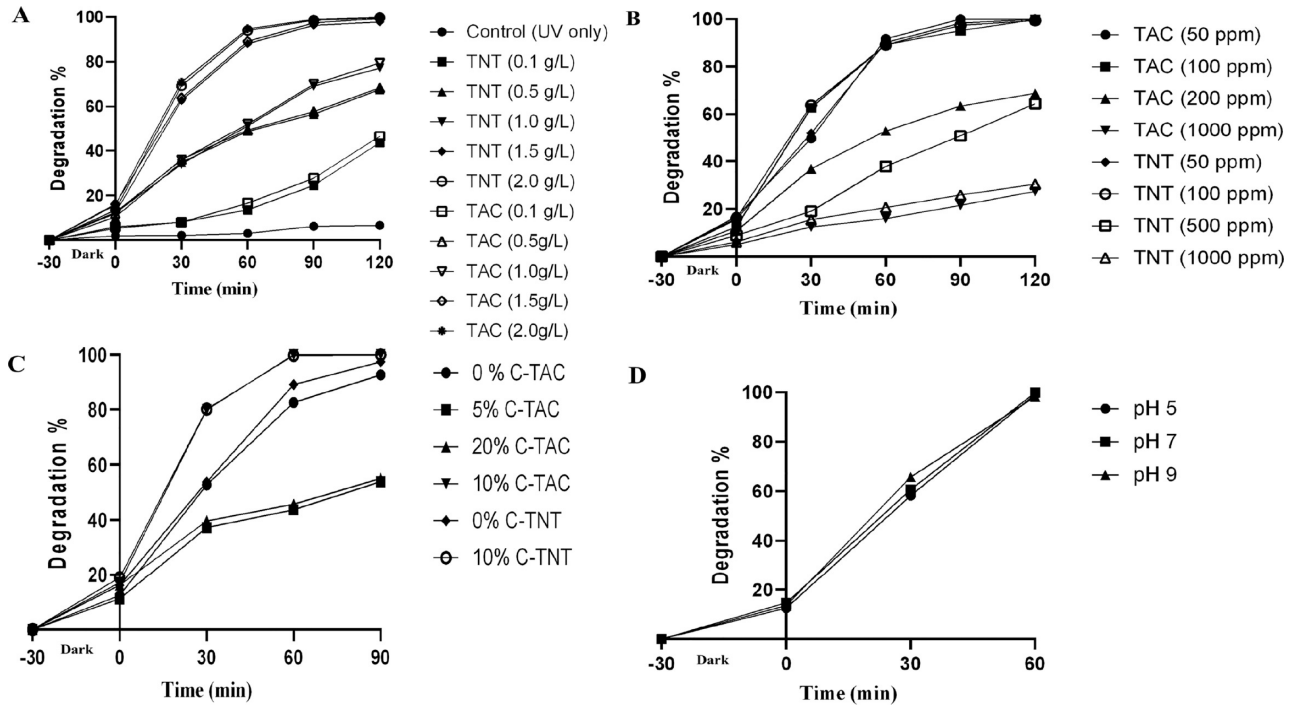

Figure 6. Effect of different parameters [(A) photocatalyst loading, (B) initial TC concentration, (C) Cu_2O concentration, and (D) pH] on photodegradation rate of TC.

of active sites for adsorption on the photocatalyst and also limited the light penetration in the reaction mixture. 100 ppm was the optimum concentration of TC used for further photodegradation study.

3.2.3. Cuprous Oxide Doping Effect. To confirm the active role of cuprous oxide in doped TiO_2 nanotubes, different concentrations of cuprous oxide (5, 10, and 20%) were coupled to get different photocatalysts and these modified forms were investigated for TC degradation. The active capacity of developed photocatalysts was evaluated in the designed photoreactor system at room temperature (25 ± 2 °C) and under visible light conditions. 100% degradation was achieved with 10% Cu_2O-doped-TiO_2 nanotubes (10% C-TAC) in 60 min as compared to non-doped TiO_2 nanotubes (TAC/TNT) (82% degradation at the same time but under UV light conditions). Therefore, the degradation efficiency was improved with decreased time (half time) to degrade the same amount of TC under visible light (Figure 6C). However, 5 and 20% doping did not enhance the degradation efficiency in visible light.

3.2.4. Effect of pH. The effect of three different pH on the degradation efficiency of the photocatalytic system was evaluated. The pH of the solution effectively plays a role in the protonation−deprotonation equilibrium of antibiotics and hydrolysis of the copper material, which further influences the free-radical oxidation and degradation of TC. The pH of the reaction mixture was adjusted to 5.0 (acidic condition), 7.0 (neutral condition), and 9.0 (basic condition) with addition of the required concentration of HCl (1 M) and NaOH (1 M). Figure 6D shows that the degradation rate of the selected photocatalyst was 100% under all tested conditions (acidic, neutral, and alkaline). Irrespective of pH, a high degradation rate of TC was observed in contrast to Safari et al. (2015),[69] who reported that the degradation rate was dependent on the initial pH of the matrix. However, at neutral pH, the degradation percentage was slightly higher than that under the acidic and basic conditions. Zhu et al. (2013) reported similar results for the neutral conditions but contrast trends for basic and acidic pH.[72] Divakaran et al. (2021) also reported acidic pH (pH 4.5) as optimum pH for TC photodegradation.[71]

3.3. Kinetics Study of Photodegradation of TC. The kinetics of photodegradation of TC by TNT/TAC (non-doped) and C-TAC/TNT (doped) photocatalyst under different conditions was investigated with the estimation of the final concentration after time t, and a graph was plotted to fit the reaction to the suitable kinetics. The Langmuir−Hinshelwood kinetics model following first-order kinetics was applied for the photocatalytic degradation of TC. Figure 7 indicates the graph

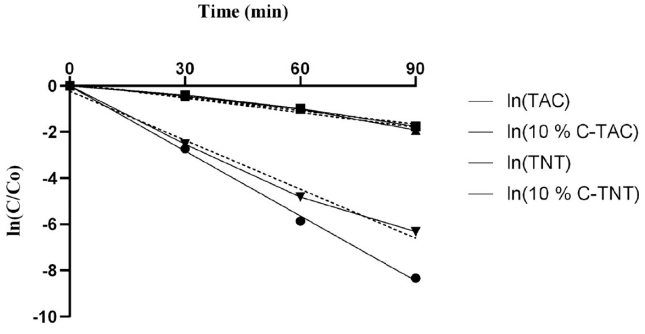

Figure 7. First-order kinetics graph of photodegradation of TC with 10% Cu_2O-doped and native photocatalysts.

of first-order degradation reaction kinetics of TC with selected photocatalysts (TAC and TNT). The rate constants of photodegradation of TC with doped photocatalysts [10% C-TNT (1.234×10^{-3} sec^{-1}) and 10% C-TAC (1.562×10^{-3} sec^{-1})] were much higher than those with the non-doped photocatalysts [TAC (3.267×10^{-4} sec^{-1}) and TNT (3.017×10^{-4} sec^{-1})].

https://doi.org/10.1021/acsomega.2c04576
ACS Omega 2022, 7, 33572−33586

3.4. Reusability and Stability of the Photocatalyst. Reusability and chemical stability are very important characteristics of the photocatalyst for its practical application on the industrial level or in wastewater treatment plants. The cost inputs are lowered with maximized reuse of the photocatalyst without interfering with the catalytic efficiency. Therefore, the recyclability of the photocatalyst was checked for six consecutive batch cycles. The photocatalyst was separated out, rinsed with deionized water, dried in a hot air oven at 50 °C, and reused for the next degradation cycle. It was observed that the photodegradation efficiency was not depleted up to five cycles, but in the sixth cycle, it was lower (85% degradation) than that of the fresh photocatalyst (100% degradation) (Figure 8). These results confirmed the reusability and stability of the photocatalyst, consistent with the reports of other researchers.[51,72−76]

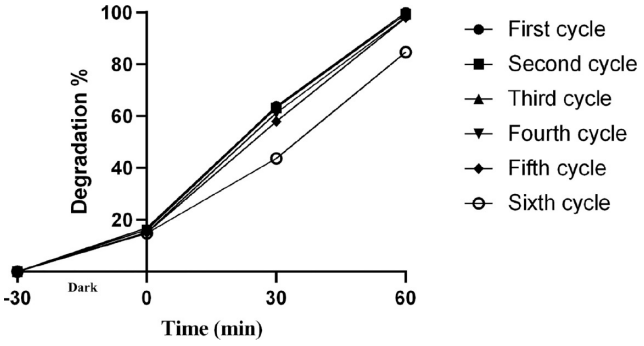

Figure 8. Reusability and stability of 10% C-TAC photocatalyst.

3.5. Photodegradation and Removal Efficiency. Photodegradation of TC over synthesized TiO_2 nanotubes was evaluated under UV and visible light irradiations. As shown in Figure 6A, in the absence of the photocatalyst, the TC concentration remained unchanged with increasing irradiation time, indicating negligible photolysis of TC without the photocatalyst. This result was similar to the results of Jiao and co-workers.[70] On the other hand, without light irradiation, TiO_2 nanotubes can adsorb TC (about 20%) and reach the adsorption equilibrium within about 30 min. Furthermore, under UV light (λ = 350 nm) irradiation over TiO_2 nanotubes, the photodegradation of TC reached up to 99.99% in 120 min and 100% in 150 min with 1.5 g of native photocatalysts (TAC and TNT) per liter. However, with cuprous oxide, this degradation was achieved within 60 min. Also, Cu_2O-doped photocatalytic degradation was carried out under visible light (absorbance range of the cuprous oxide-doped photocatalyst) conditions, while UV light (absorbance range of the native photocatalyst) conditions were applied for the native photocatalyst. Wu and coworkers were the first to report on the photodegradation of TC by the TiO_2-based photocatalyst under visible light, where only 25.1% removal efficiency was achieved.[77] However, they were able to achieve 66.2 and 59.6% removal of TC with black anatase TiO_2 and N-doped TiO_2, respectively.[78] Similarly, Lv et al. (2021) were able to degrade more than 99% TC in 20 min with IO−TiO_2−CdS (inverse opal TiO_2 and cadmium sulfide) photocatalyst,[79] while with Cu-doped TiO_2−SiO_2 photocatalyst, 98% of doxycycline was degraded.[80] Most of the researchers used the TiO_2-based nanoparticles (Table 2), but in this study, TiO_2 nanotubes coupled with Cu_2O were used, which enhanced the photodegradation rate in respect of degradation percentage (100%) and time (60 min) and the higher initial concentration (100 ppm) with environment friendly non-toxic and faster photodegradation of TC.

3.6. Photodegradation Mechanism. In the presence of a suitable light energy source (equal to or more than the band gap energy), electrons are excited from the valance band to the conduction band of TiO_2 nanotubes to create valance band holes (positive charge carriers) and conduction band electrons (negative charge carriers). These electron−hole pairs recombine and are scavenged by other oxidizing species to produce different reactive oxygen species which further degrade the target pollutant (TC) on the surface of the photocatalyst (Figure 9B).

Photodegradation of TC and the formation of different intermediates during transformation were identified by LC−MS analysis (Figure S3A,B). The isotopic peaks of TC (m/z:

Table 2. Comparisons of the TiO_2-Based Photodegradation Studies of TC

photocatalyst	photon energy source	treatment time (minutes)	degradation efficiency (%)	target antibiotic initial concentration (mg/L)	toxicity evaluation of degraded products	references
White TiO_2 nanoparticles	visible	120	25.1	10	no evaluation	81
N-doped TiO_2 nanoparticles	visible	120	66.2	10	no evaluation	78
TiO_2 on magnetic activated carbon	UV and ultrasound	180	93	10	no evaluation	82
TiO_2−ferroferric oxide nanoparticles on magnetic activated carbon	UV	60	96	60	no evaluation	83
TiO_2 doped with acetylene black and persulfate	visible	120	93.3	30	80% reduction in toxicity	84
TiO_2 nanoparticles on CuO sheets	UV	90	95	50	no evaluation	85
TiO_2 nanosheet-impregnated carbon	visible adsorption	60	93	50	no evaluation	86
palygorskite-supported Cu_2O−TiO_2	solar	240	88.1	30	no evaluation	87
AgBr−TiO_2−Pal	visible	120	90	10	no evaluation	88
5% dysprosium-doped $Bi_4V_2O_{11}$ nanoparticles	visible	120	95	10	no evaluation	89
Au−TiO_2 nanocomposites	visible	120	75	10	no evaluation	90
g-C_3N_4/TiO_2	visible	90	88.4	10	no evaluation	91
TiO_2/$BiVO_2$/rGO	visible	120	96.1	10	no evaluation	92
Cu_2O coupled with TiO_2 nanotubes	visible	60	100	100	toxicity-free photodegradation	this study

https://doi.org/10.1021/acsomega.2c04576
ACS Omega 2022, 7, 33572−33586

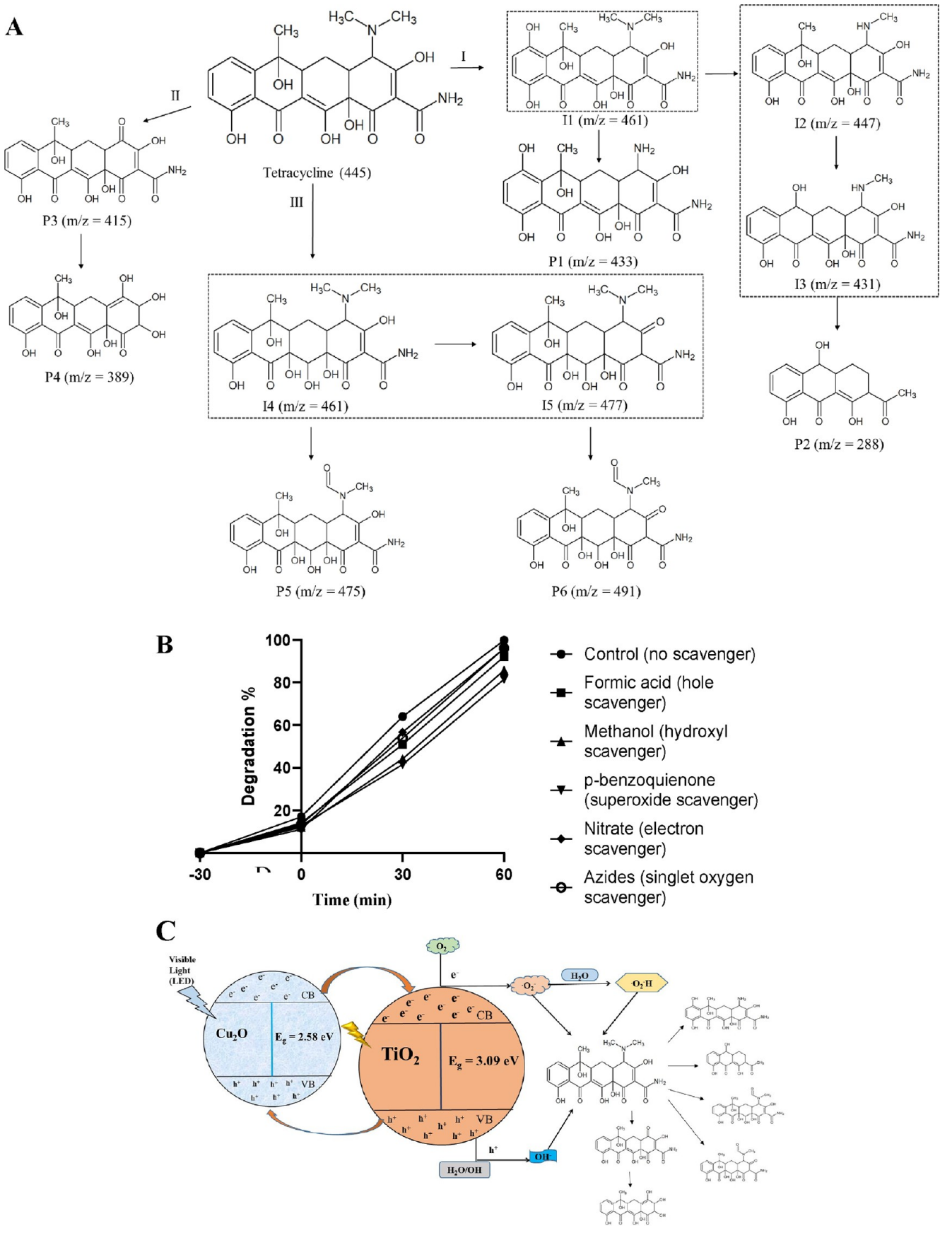

Figure 9. (A) Proposed pathways of photodegradation of TC; (B) effect of different scavengers on the photodegradation rate of TC and (C) proposed mechanism of photocatalysis (involvement of different reactive species) of TC.

https://doi.org/10.1021/acsomega.2c04576
ACS Omega 2022, 7, 33572−33586

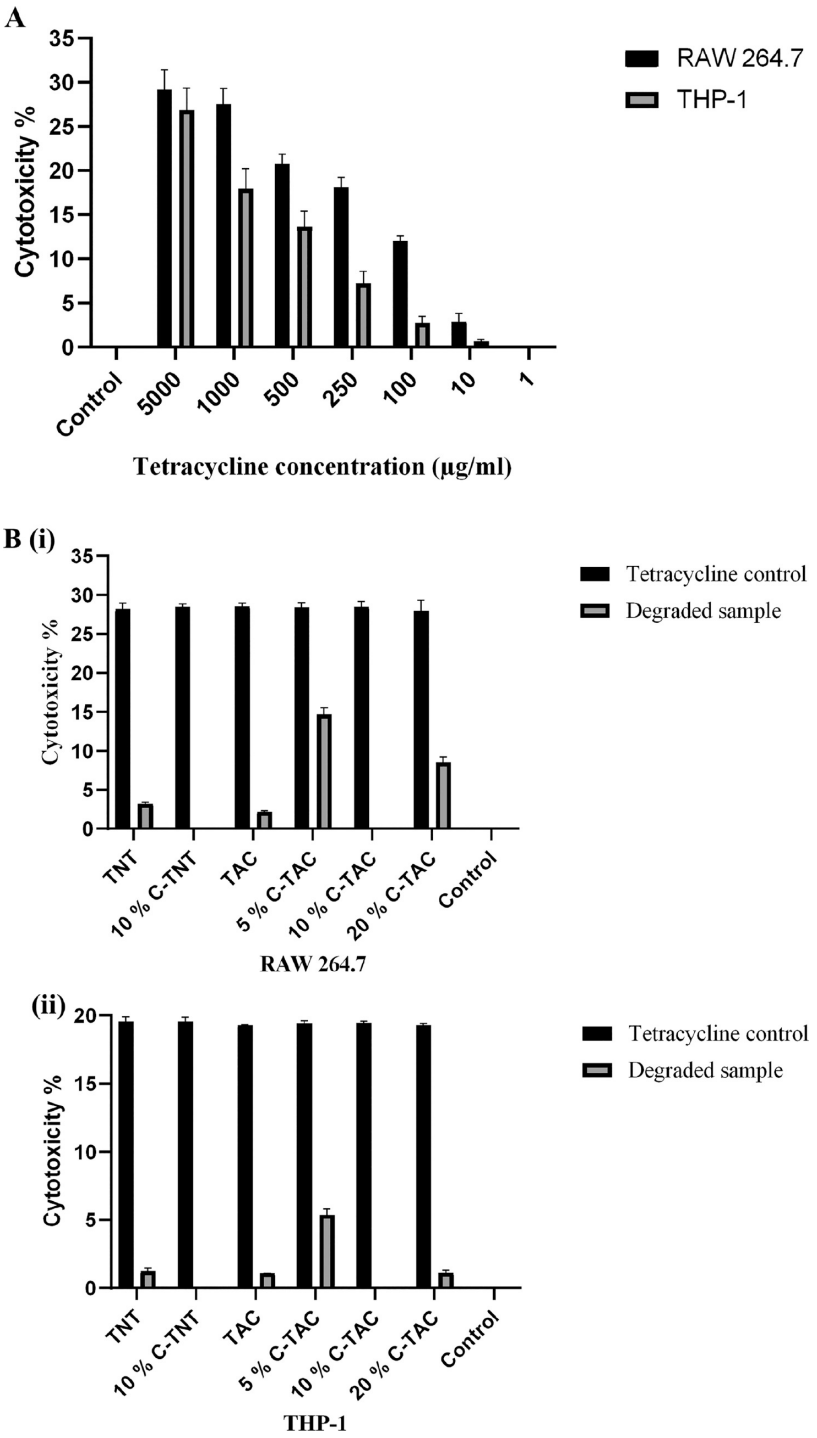

Figure 10. Toxicity testing of different TC concentrations (A) and photodegraded samples (B) of TC on RAW 264.7 (i) and THP-1 cell lines (ii).

445.1567, 447.1361, and 443.1413) with high intensity were observed at the start of the photodegradation experiment samples (Figure S3A), and the intensity of TC (m/z—445.1565) was decreased during the photodegradation with the formation of other transformed products (Figure S3B). The MS peaks shown in the degraded samples suggested that there are mainly three sites of attack of different reactive species. The benzene ring of TC ($m/z = 445$) is hydroxylated by the hydroxyl radicals ($^{\bullet}OH$) to produce an intermediate isomer I1 (m/z = 461). This intermediate isomer in further attacked by conduction band holes (h^+) at the N-dimethyl group to produce product P1 (m/z = 433), which is further transformed into product P2 ($m/z = 288$) via two more intermediates (I2 and I3). Similar transformed products of TC were reported previously.[93,94] Also, the N-dimethyl group of TC can be directly oxidized into the carbonyl group to produce product P3 (m/z = 415). The C−N bond of TC is substituted by the hydroxyl group to produce product P4 (m/z = 389). Lai et al. (2021) reported the same transformed product of TC.[95,96] The double bonds of TC were attacked by the hydroxyl radicals to produce intermediate isomers I4 ($m/z = 461$), which are further oxidized to produce another intermediate I5 ($m/z = 477$). Intermediates

https://doi.org/10.1021/acsomega.2c04576
ACS Omega 2022, 7, 33572−33586

I4 and I5 are further oxidized by the hydroxyl radicles to generate product P5 (m/z = 475) and P6 (m/z = 491), respectively. Similar products were reported by other researchers.[97,98] The LC−MS data were analyzed with thermoscientific Compound Discoverer 3.1, and the results of photodegraded samples and the photodegradation pathway of TC were proposed (Figure 9A).

Different scavengers (sodium nitrate, sodium azide, *p*-benzoquinone, *t*-butanol, and ammonium oxalate) were used to verify the mechanism of photodegradation of TC, and also, the roles of different radicals (VB_e^-,$^\bullet O_2$, $^\bullet O_2^-$/$^\bullet O_2H$, $^\bullet OH$, CB_{h+}) were identified. In the presence of specific scavengers, the maximum decrease in degradation percentage was observed with *p*-benzoquinone (superoxide scavenger), followed by methanol (hydroxyl scavenger) and formic acid (conduction band hole scavenger) (Figure 9B). It was observed that upon excitation of electrons, both valance band electrons and conduction band holes play a role in photodegradation of TC, but the most involved reactive species in photodegradation was the superoxide radical ($^\bullet O_2^-$ and $^\bullet O_2H$), followed by hydroxyl radicals ($^\bullet OH$) and conduction band holes (CB_{h+}). The least involved reactive species in photodegradation of TC were valance band electrons and singlet oxygen (VB_e^- and O_2). Similar results about the involvement of superoxide radicals were reported by other researchers.[71,76,84,99−101] The role of hydroxyl radicals in the photodegradation of TC was similar to other studies.[76,102] The proposed photodegradation mechanism of TC with the developed photocatalyst is shown in Figure 9C.

3.7. Toxicity Analysis of Native and Degraded Products. MTT assay was performed to determine the cytotoxicity of TC and degraded products as the absorbance data of the MTT assay were directly related to the viability of the active cells.[103,104] The MTT assay of native TC in triplicates of different concentrations (1, 10, 100, 250, 500, 1000, and 5000 μg/mL) on RAW 264.7 and THP-1 was used to test its toxicity. Bettany et al. (1998) reported that TC causes apoptosis and cell death of mouse macrophage cell lines (RAW 264).[104] Figure 10A shows that TC exhibited higher toxicity against RAW 264.7 cells as compared to THP-1. This variation was more for lower concentrations (10, 100, and 250 μg/mL) of the antibiotic than for higher concentrations (1000 and 5000 μg/mL). However, 1 μg/mL of TC solution did not show toxicity against both the cell lines. The toxicity percentage is dependent on TC dose and increased with an increase in the concentration of TC. Similar trends of dose-dependent toxicity of TC were described in other studies.[103,105] The degraded sample of each photocatalytic reaction performed in triplicates was used for toxicity testing against the selected cell lines. The toxicity percentage of TC and its degraded products showed a negative correlation [RAW 264.7: R^2 (−0.932), *p*-value (0.01) and THP-1: R^2 (−0.931), *p*-value (0.01)] with the degradation rate, and it confirmed the degradation of the antibiotic and loss of its activity (Figure 10B(i,ii)). Most of the researchers used fish and other cell lines for testing of toxicity of antimicrobials, and they observed various adverse genetic mutations and cytotoxic, genotoxic, and transgenerational effects on the developing cells.[105−110] For its high toxicity and mutation and modulation effects, TC is nowadays used for the study of different tumor cell lines including mammalian cell lines (hepatic, monocytes, macrophages).[15,111−114] Itoh et al. (2021) reported that antimicrobial compounds like TC modulate the immune cells (THP-1), while Liu et al. (2019) confirmed the cytotoxicity of TC present in soil samples against human cell lines (HL-7702).[15,115]

4. CONCLUSIONS

Being the second most used antibiotic, TC is continuously discharged in the aquatic system, and because of its low metabolism rate, most of the used TC (≥95%) is excreted out in the biologically active form. The presence of TC in the aquatic system had many adverse effects on non-target organisms including the most scientific concern of antimicrobial resistance. TC is sensitive to light, but only photolysis may not eliminate these from the aquatic system because of the limiting effect of light penetration or the presence of a high concentration of the antibiotic. For this, heterostructured Cu_2O-TiO_2 nanotubes were used for the complete photodegradation of TC. With Cu_2O-TiO_2 nanotube-based photocatalytic degradation of TC over other photodegradations, the concluding remarks are as follows:

- With cuprous oxide coupling, the band gap energy of the photocatalyst was reduced up to 2.58 eV (10% cuprous oxide doping) and the red shift was observed with photoexcitation of electrons in the visible range of light.
- With a greater surface area, with Cu_2O-TiO_2 nanotubes, 100% degradation of TC was achieved within 60 min of visible light irradiation.
- The photodegradation rate was found to be dependent on the photocatalyst dose and initial concentration of TC but independent of pH conditions.
- pH independency lowers the cost inputs of TC degradation and facilitates its effective use in the original water matrix.
- The selected photocatalyst had high chemical stability and could be effectively reused.
- Toxicity studies confirmed the negligible toxicity of almost all the degraded and transformed products to both the cell lines (RAW 264.7 and THP-1).
- Thus, the selected photocatalyst showed low-cost, energy-efficient, faster, and environment-friendly photodegradation of TC without any ecotoxicity of degraded effluents.

■ ASSOCIATED CONTENT

Supporting Information

The Supporting Information is available free of charge at https://pubs.acs.org/doi/10.1021/acsomega.2c04576.

Schematic diagram and working design of the photoreactor system; brief methodology followed for cytotoxicity testing of parent antibiotics and transformed products; and LC−MS of the sample at the start of the photodegradation experiment and LC−MS of a photodegraded sample of TC (PDF)

■ AUTHOR INFORMATION

Corresponding Author

Kashyap Kumar Dubey − *Bioprocess Engineering Laboratory, School of Biotechnology, Jawaharlal Nehru University, New Delhi 110067, India;* orcid.org/0000-0002-4204-009X; Phone: +919996122280; Email: kashyapdubey@gmail.com

Authors

Manisha Sharma − *Department of Biotechnology, Central University of Haryana, Mahendergarh, Haryana 123031, India*

https://doi.org/10.1021/acsomega.2c04576
ACS Omega 2022, 7, 33572−33586

Mrinal Kanti Mandal − *Department of Chemical Engineering, National Institute of Technology, Durgapur, West Bengal 713209, India*
Shailesh Pandey − *Department of Chemical Engineering, National Institute of Technology, Durgapur, West Bengal 713209, India*
Ravi Kumar − *Department of Biotechnology, Central University of Haryana, Mahendergarh, Haryana 123031, India*

Complete contact information is available at: https://pubs.acs.org/10.1021/acsomega.2c04576

Notes

The authors declare no competing financial interest.

■ ACKNOWLEDGMENTS

The author M.S. (09/1152/(0007)/2017-EMR-I) would like to acknowledge the Council of Scientific and Industrial Research for providing fellowship. The authors would like to acknowledge Dr. Vinod Yadav (Assistant Professor, Department of Microbiology, Central University of Haryana) and Dr. Ved Prakash Dwivedi (Group leader, Immunobiology Group, International Centre for Genetic Engineering and Biotechnology) for providing cell lines and guidance in cytotoxicity experiments.

■ REFERENCES

(1) Cheng, D.; Ngo, H. H.; Guo, W.; Chang, S. W.; Nguyen, D. D.; Liu, Y.; Wei, Q.; Wei, D. A critical review on antibiotics and hormones in swine wastewater: Water pollution problems and control approaches. *J. Hazard. Mater.* **2020**, *387*, 121682.
(2) Luo, T.; Feng, H.; Tang, L.; Lu, Y.; Tang, W.; Chen, S.; Yu, J.; Xie, Q.; Ouyang, X.; Chen, Z. Efficient degradation of tetracycline by heterogeneous electro-Fenton process using Cu-doped Fe@ Fe_2O_3: Mechanism and degradation pathway. *Chem. Eng. J.* **2020**, *382*, 122970.
(3) US Food and Drug Administration. *Summary Report on Antimicrobials Sold or Distributed for Use in Food-Producing Animals*, 2017.
(4) Khan, N. A.; Ahmed, S.; Farooqi, I. H.; Ali, I.; Vambol, V.; Changani, F.; Yousefi, M.; Vambol, S.; Khan, S. U.; Khan, A. H. Occurrence, Sources and Conventional Treatment Techniques for various antibiotics present in hospital wastewaters: A critical review. *TrAC, Trends Anal. Chem.* **2020**, *129*, 115921.
(5) Baietto, L.; Corcione, S.; Pacini, G.; Perri, G.; D'Avolio, A.; De Rosa, F. A 30-years review on pharmacokinetics of antibiotics: is the right time for pharmacogenetics? *Curr. Drug Metab.* **2014**, *15*, 581−598.
(6) Xiong, W.; Sun, Y.; Zhang, T.; Ding, X.; Li, Y.; Wang, M.; Zeng, Z. Antibiotics, antibiotic resistance genes, and bacterial community composition in fresh water aquaculture environment in China. *Microb. Ecol.* **2015**, *70*, 425−432.
(7) Sharma, M.; Kumar, K.; Dubey, K. K. Disposal of unused antibiotics as household waste: A social driver of antimicrobial resistance. *Environ. Qual. Manage.* **2021**, *30*, 127.
(8) Daouk, S.; Chèvre, N.; Vernaz, N.; Bonnabry, P.; Dayer, P.; Daali, Y.; Fleury-Souverain, S. Prioritization methodology for the monitoring of active pharmaceutical ingredients in hospital effluents. *J. Environ. Manage.* **2015**, *160*, 324−332.
(9) Kim, C.; Ryu, H.-d.; Chung, E. G.; Kim, Y.; Lee, J.-k. A review of analytical procedures for the simultaneous determination of medically important veterinary antibiotics in environmental water : Sample preparation , liquid chromatography , and mass spectrometry. *J. Environ. Manage.* **2018**, *217*, 629−645.
(10) Abdi, J.; Hadipoor, M.; Hadavimoghaddam, F.; Hemmati-Sarapardeh, A. Estimation of tetracycline antibiotic photodegradation from wastewater by heterogeneous metal-organic frameworks photocatalysts. *Chemosphere* **2022**, *287*, 132135.
(11) Gopal, G.; Alex, S. A.; Chandrasekaran, N.; Mukherjee, A. A review on tetracycline removal from aqueous systems by advanced treatment techniques. *RSC Adv.* **2020**, *10*, 27081−27095.
(12) aus der Beek, T.; Weber, F. A.; Bergmann, A.; Hickmann, S.; Ebert, I.; Hein, A.; Küster, A. Pharmaceuticals in the environment—Global occurrences and perspectives. *Environ. Toxicol. Chem.* **2016**, *35*, 823−835.
(13) Sharma, M.; Yadav, A.; Dubey, K. K.; Tipple, J.; Das, D. B. Decentralized systems for the treatment of antimicrobial compounds released from hospital aquatic wastes. *Sci. Total Environ.* **2022**, *840*, 156569.
(14) Bengtsson-Palme, J.; Larsson, D. J. Concentrations of antibiotics predicted to select for resistant bacteria: proposed limits for environmental regulation. *Environ. Int.* **2016**, *86*, 140−149.
(15) Liu, D.; Lu, L.; Wang, M.; Hussain, B.; Tian, S.; Luo, W.; Zhou, J.; Yang, X. Tetracycline uptake by pak choi grown on contaminated soils and its toxicity in human liver cell line HL-7702. *Environ. Pollut.* **2019**, *253*, 312−321.
(16) Cycoń, M.; Mrozik, A.; Piotrowska-Seget, Z. Antibiotics in the soil environment—degradation and their impact on microbial activity and diversity. *Front. Microbiol.* **2019**, *10*, 338.
(17) Singh, R.; Singh, A. P.; Kumar, S.; Giri, B. S.; Kim, K.-H. Antibiotic resistance in major rivers in the world: a systematic review on occurrence, emergence, and management strategies. *J. Clean. Prod.* **2019**, *234*, 1484−1505.
(18) Khan, F. A.; Söderquist, B.; Jass, J. Prevalence and diversity of antibiotic resistance genes in Swedish aquatic environments impacted by household and hospital wastewater. *Front. Microbiol.* **2019**, *10*, 688.
(19) Pedrazzani, R.; Bertanza, G.; Brnardić, I.; Cetecioglu, Z.; Dries, J.; Dvarionienė, J.; García-Fernández, A. J.; Langenhoff, A.; Libralato, G.; Lofrano, G.; Škrbić, B.; Martínez-López, E.; Meriç, S.; Pavlović, D. M.; Papa, M.; Schröder, P.; Tsagarakis, K. P.; Vogelsang, C. Opinion paper about organic trace pollutants in wastewater: Toxicity assessment in a European perspective. *Sci. Total Environ.* **2019**, *651*, 3202−3221.
(20) Kumar, M.; Jaiswal, S.; Sodhi, K. K.; Shree, P.; Singh, D. K.; Agrawal, P. K.; Shukla, P. Antibiotics bioremediation: Perspectives on its ecotoxicity and resistance. *Environ. Int.* **2019**, *124*, 448−461.
(21) Yang, Q.; Gao, Y.; Ke, J.; Show, P. L.; Ge, Y.; Liu, Y.; Guo, R.; Chen, J. Antibiotics: An overview on the environmental occurrence, toxicity, degradation, and removal methods. *Bioengineered* **2021**, *12*, 7376−7416.
(22) Lu, Z.-Y.; Ma, Y.-L.; Zhang, J.-T.; Fan, N.-S.; Huang, B.-C.; Jin, R.-C. J. A critical review of antibiotic removal strategies: Performance and mechanisms. *J. Water Process Eng.* **2020**, *38*, 101681.
(23) Singh, S.; Faraz, M.; Khare, N. Recent advances in semiconductor−graphene and semiconductor−ferroelectric/ferromagnetic nanoheterostructures for efficient hydrogen generation and environmental remediation. *ACS Omega* **2020**, *5*, 11874−11882.
(24) Wu, M.-H.; Que, C.-J.; Xu, G.; Sun, Y.-F.; Ma, J.; Xu, H.; Sun, R.; Tang, L. Occurrence, fate and interrelation of selected antibiotics in sewage treatment plants and their receiving surface water. *Ecotoxicol. Environ. Saf.* **2016**, *132*, 132−139.
(25) Zrnčić, M.; Babić, S.; Mutavdžić Pavlović, D. Determination of thermodynamic pKa values of pharmaceuticals from five different groups using capillary electrophoresis. *J. Sep. Sci.* **2015**, *38*, 1232−1239.
(26) Ali, T.; Tripathi, P.; Azam, A.; Raza, W.; Ahmed, A. S.; Ahmed, A.; Muneer, M. Photocatalytic performance of Fe-doped TiO_2 nanoparticles under visible-light irradiation. *Mater. Res. Express* **2017**, *4*, 015022.
(27) Minetto, D.; Volpi Ghirardini, A. V.; Libralato, G. Saltwater ecotoxicology of Ag, Au, CuO, TiO_2, ZnO and C60 engineered nanoparticles: an overview. *Environ. Int.* **2016**, *92*−*93*, 189−201.
(28) Serna-Galvis, E. A.; Silva-Agredo, J.; Giraldo-Aguirre, A. L.; Flórez-Acosta, O. A.; Torres-Palma, R. A. High frequency ultrasound as a selective advanced oxidation process to remove penicillinic antibiotics and eliminate its antimicrobial activity from water. *Ultrason. Sonochem.* **2016**, *31*, 276−283.

(29) Clark, J. A.; Yang, Y.; Ramos, N. C.; Hillhouse, H. W. Selective oxidation of pharmaceuticals and suppression of perchlorate formation during electrolysis of fresh human urine. *Water Res.* **2021**, *198*, 117106.
(30) Li, W.; Liu, Y.; Duan, J.; van Leeuwen, J.; Saint, C. P. UV and UV/H_2O_2 treatment of diazinon and its influence on disinfection byproduct formation following chlorination. *Chem. Eng. J.* **2015**, *274*, 39−49.
(31) Ji, Y.; Pan, Z.; Yuan, D.; Lai, B. Advanced Treatment of the Antibiotic Production Wastewater by Ozone/Zero-Valent Iron Process. *Clean* **2018**, *46*, 1700666.
(32) Lakshmi, K.; Varadharajan, V.; Kadirvelu, K. G. Photocatalytic Decontamination of Organic Pollutants Using Advanced Materials. *Modern Age Waste Water Problems*; Springer, 2020; pp 195−212.
(33) Lofrano, G.; Pedrazzani, R.; Libralato, G.; Carotenuto, M. Advanced Oxidation Processes for Antibiotics Removal: A Review. *Curr. Org. Chem.* **2017**, *21*, 1054−1067.
(34) Koe, W. S.; Lee, J. W.; Chong, W. C.; Pang, Y. L.; Sim, L. C. An overview of photocatalytic degradation: photocatalysts, mechanisms, and development of photocatalytic membrane. *Environ. Sci. Pollut. Res.* **2020**, *27*, 2522−2565.
(35) Šuligoj, A.; Kete, M.; Černigoj, U.; Fresno, F.; Lavrenčič Štangar, U. L. Synergism in TiO_2 photocatalytic ozonation for the removal of dichloroacetic acid and thiacloprid. *Environ. Res.* **2021**, *197*, 110982.
(36) Khosya, M.; Faraz, M.; Khare, N. Enhanced photocatalytic reduction of hexavalent chromium by using piezo-photo active calcium bismuth oxide ferroelectric nanoflakes. *New J. Chem.* **2022**, *46*, 12244−12251.
(37) Sharma, M.; Yadav, A.; Mandal, M.; Dubey, K. TiO_2 based photocatalysis: a valuable approach for the removal of pharmaceuticals from aquatic environment. *Int. J. Sci. Technol.* **2022**, 1−16.
(38) Lofrano, G.; Libralato, G.; Casaburi, A.; Siciliano, A.; Iannece, P.; Guida, M.; Pucci, L.; Dentice, E. F.; Carotenuto, M. Municipal wastewater spiramycin removal by conventional treatments and heterogeneous photocatalysis. *Sci. Total Environ.* **2018**, *624*, 461−469.
(39) Carotenuto, M.; Lofrano, G.; Siciliano, A.; Aliberti, F.; Guida, M. TiO_2 photocatalytic degradation of caffeine and ecotoxicological assessment of oxidation by-products. *Global NEST J.* **2014**, *16*, 463.
(40) Truong, H. B.; Bae, S.; Cho, J.; Hur, J. Advances in application of g−C_3N_4−based materials for treatment of polluted water and wastewater via activation of oxidants and photoelectrocatalysis: A comprehensive review. *Chemosphere* **2022**, *286*, 131737.
(41) Atacan, K.; Güy, N.; Özacar, M. Recent advances in photocatalytic coatings for antimicrobial surfaces. *Curr. Opin. Chem. Eng.* **2022**, *36*, 100777.
(42) Ren, G.; Han, H.; Wang, Y.; Liu, S.; Zhao, J.; Meng, X.; Li, Z. Recent advances of photocatalytic application in water treatment: A review. *Nanomaterials* **2021**, *11*, 1804.
(43) Guo, R.-t.; Wang, J.; Bi, Z.-x.; Chen, X.; Hu, X.; Pan, W.-g. Recent advances and perspectives of g−C_3N_4−based materials for photocatalytic dyes degradation. *Chemosphere* **2022**, *295*, 133834.
(44) Guo, Z.; Zheng, J.; Li, B.; Da, Z.; Meng, M. Fabrication of mixed matrix membranes blending with the TiO_2/Bi_3O_4Cl 2D/2D heterojunction for photocatalytic degradation of tetracycline. *Appl. Surf. Sci.* **2022**, *574*, 151549.
(45) Zhao, Y.; Li, Y.; Sun, L. Recent advances in photocatalytic decomposition of water and pollutants for sustainable application. *Chemosphere* **2021**, *276*, 130201.
(46) Zhao, Y.; Li, Z.; Wei, J.; Li, X.; Shi, H.; Cao, B.; Fan, J. Efficient photodegradation of cefixime catalyzed by a direct Z-scheme CQDs-BiOBr/CN composite: Performance, toxicity evaluation and photocatalytic mechanism. *Chemosphere* **2022**, *292*, 133430.
(47) Zhu, X.; Guo, F.; Pan, J.; Sun, H.; Gao, L.; Deng, J.; Zhu, X.; Shi, W. Fabrication of visible-light-response face-contact $ZnSnO_3$@ gC_3N_4 core−shell heterojunction for highly efficient photocatalytic degradation of tetracycline contaminant and mechanism insight. *J. Mater. Sci.* **2021**, *56*, 4366−4379.
(48) Bayan, E.; Pustovaya, L.; Volkova, M. Recent advances in TiO_2-based materials for photocatalytic degradation of antibiotics in aqueous systems. *Environ. Technol. Innovation* **2021**, *24*, 101822.
(49) Perović, K.; dela Rosa, F. M.; Kovačić, M.; Kušić, H.; Štangar, U. L.; Fresno, F.; Dionysiou, D. D.; Loncaric Bozic, A. Recent achievements in development of TiO_2-based composite photocatalytic materials for solar driven water purification and water splitting. *Materials* **2020**, *13*, 1338.
(50) Sharma, D.; Faraz, M.; Kumar, D.; Takhar, D.; Birajdar, B.; Khare, N. Visible light activated V_2O_5/rGO nanocomposite for enhanced photodegradation of methylene blue dye and photoelectrochemical water splitting. *Inorg. Chem. Commun.* **2022**, *142*, 109657.
(51) Babu, S. G.; Karthik, P.; John, M. C.; Lakhera, S. K.; Ashokkumar, M.; Khim, J.; Neppolian, B. Synergistic effect of sono-photocatalytic process for the degradation of organic pollutants using CuO-TiO_2/rGO. *Ultrason. Sonochem.* **2019**, *50*, 218−223.
(52) Bathla, A.; Rather, R. A.; Poonia, T.; Pal, B. Morphology dependent photocatalytic activity of CuO/CuO−TiO_2 nanocatalyst for degradation of methyl orange under sunlight. *J. Nanosci. Nanotechnol.* **2020**, *20*, 3123−3130.
(53) Khanmohammadi, M.; Shahrouzi, J. R.; Rahmani, F. Insights into mesoporous MCM-41-supported titania decorated with CuO nanoparticles for enhanced photodegradation of tetracycline antibiotic. *Environ. Sci. Pollut. Res.* **2021**, *28*, 862−879.
(54) Yu, X.; Zhang, J.; Zhang, J.; Niu, J.; Zhao, J.; Wei, Y.; Yao, B. Photocatalytic degradation of ciprofloxacin using Zn-doped Cu_2O particles: Analysis of degradation pathways and intermediates. *Chem. Eng. J.* **2019**, *374*, 316−327.
(55) Kasuga, T.; Hiramatsu, M.; Hoson, A.; Sekino, T.; Niihara, K. Formation of titanium oxide nanotube. *Langmuir* **1998**, *14*, 3160−3163.
(56) Manjunatha, K. N.; Paul, S. Investigation of optical properties of nickel oxide thin films deposited on different substrates. *Appl. Surf. Sci.* **2015**, *352*, 10−15.
(57) Li, D.; Song, H.; Meng, X.; Shen, T.; Sun, J.; Han, W.; Wang, X. Effects of particle size on the structure and photocatalytic performance by alkali-treated TiO_2. *Nanomaterials* **2020**, *10*, 546.
(58) Bohm, D.; Stachel, C.; Gowik, P. Multi-method for the determination of antibiotics of different substance groups in milk and validation in accordance with Commission Decision 2002/657/EC. *J. Chromatogr. A* **2009**, *1216*, 8217−8223.
(59) Yadav, A.; Mandal, M. K.; Dubey, K. K. In vitro cytotoxicity study of cyclophosphamide, etoposide and paclitaxel on monocyte macrophage cell line raw 264.7. *Indian J. Microbiol.* **2020**, *60*, 511−517.
(60) Zavala, M. Á. L.; Morales, S. A. L.; Ávila-Santos, M. Synthesis of stable TiO_2 nanotubes: effect of hydrothermal treatment, acid washing and annealing temperature. *Heliyon* **2017**, *3*, No. e00456.
(61) Sarteep, Z.; Ebrahimian Pirbazari, A.; Aroon, M. A. Silver doped TiO_2 nanoparticles: preparation, characterization and efficient degradation of 2, 4-dichlorophenol under visible light. *J. Water Environ. Nanotechnol.* **2016**, *1*, 135−144.
(62) Ba-Abbad, M. M.; Kadhum, A. A. H.; Mohamad, A. B.; Takriff, M. S.; Sopian, K. Synthesis and catalytic activity of TiO_2 nanoparticles for photochemical oxidation of concentrated chlorophenols under direct solar radiation. *Int. J. Electrochem. Sci* **2012**, *7*, 4871−4888.
(63) Salma, A.; Thoröe-Boveleth, S.; Schmidt, T. C.; Tuerk, J. Dependence of transformation product formation on pH during photolytic and photocatalytic degradation of ciprofloxacin. *J. Hazard. Mater.* **2016**, *313*, 49−59.
(64) Suwarnkar, M.; Dhabbe, R.; Kadam, A.; Garadkar, K. Enhanced photocatalytic activity of Ag doped TiO_2 nanoparticles synthesized by a microwave assisted method. *Ceram. Int.* **2014**, *40*, 5489−5496.
(65) Varma, K.; Gandhi, V.; Tayade, R.; Shukla, A.; Bharatiya, B.; Joshi, P. Photocatalytic Degradation of Levofloxacin by Cu doped TiO_2 under Visible LED Light. *Adv. Wastewater Treat. II* **2021**, *102*, 182−198.
(66) Mathew, S.; Ganguly, P.; Rhatigan, S.; Kumaravel, V.; Byrne, C.; Hinder, S. J.; Bartlett, J.; Nolan, M.; Pillai, S. C. Cu-doped TiO_2: visible light assisted photocatalytic antimicrobial activity. *Appl. Sci.* **2018**, *8*, 2067.

https://doi.org/10.1021/acsomega.2c04576
ACS Omega 2022, 7, 33572−33586

(67) Palominos, R. A.; Mondaca, M. A.; Giraldo, A.; Peñuela, G.; Pérez-Moya, M.; Mansilla, H. D. Photocatalytic oxidation of the antibiotic tetracycline on TiO_2 and ZnO suspensions. *Catal. Today* **2009**, *144*, 100−105.
(68) Reyes, C.; Fernández, J.; Freer, J.; Mondaca, M. A.; Zaror, C.; Malato, S.; Mansilla, H. D. Degradation and inactivation of tetracycline by TiO_2 photocatalysis. *J. Photochem. Photobiol. A* **2006**, *184*, 141−146.
(69) Safari, G.; Hoseini, M.; Seyedsalehi, M.; Kamani, H.; Jaafari, J.; Mahvi, A. Photocatalytic degradation of tetracycline using nanosized titanium dioxide in aqueous solution. *Int. J. Environ. Sci. Technol.* **2015**, *12*, 603−616.
(70) Jiao, S.; Zheng, S.; Yin, D.; Wang, L.; Chen, L. Aqueous photolysis of tetracycline and toxicity of photolytic products to luminescent bacteria. *Chemosphere* **2008**, *73*, 377−382.
(71) Divakaran, K.; Baishnisha, A.; Balakumar, V.; Perumal, K. N.; Meenakshi, C.; Kannan, R. S. Photocatalytic degradation of tetracycline under visible light using TiO_2@ sulfur doped carbon nitride nanocomposite synthesized via in-situ method. *J. Environ. Chem. Eng.* **2021**, *9*, 105560.
(72) Zhu, X.-D.; Wang, Y.-J.; Sun, R.-J.; Zhou, D.-M. Photocatalytic degradation of tetracycline in aqueous solution by nanosized TiO_2. *Chemosphere* **2013**, *92*, 925−932.
(73) Nekooie, R.; Shamspur, T.; Mostafavi, A. Novel CuO/TiO_2/PANI nanocomposite: Preparation and photocatalytic investigation for chlorpyrifos degradation in water under visible light irradiation. *J. Photochem. Photobiol. A* **2021**, *407*, 113038.
(74) Affam, A. C.; Chaudhuri, M. Degradation of pesticides chlorpyrifos, cypermethrin and chlorothalonil in aqueous solution by TiO_2 photocatalysis. *J. Environ. Manage.* **2013**, *130*, 160−165.
(75) Bouyarmane, H.; El Bekkali, C.; Labrag, J.; Es-saidi, I.; Bouhnik, O.; Abdelmoumen, H.; Laghzizil, A.; Nunzi, J.; Robert, D. Photocatalytic degradation of emerging antibiotic pollutants in waters by TiO_2/Hydroxyapatite nanocomposite materials. *Surf. Interfaces* **2021**, *24*, 101155.
(76) Zhang, B.; He, X.; Yu, C.; Liu, G.; Ma, D.; Cui, C.; Yan, Q.; Zhang, Y.; Zhang, G.; Ma, J. Degradation of tetracycline hydrochloride by ultrafine TiO_2 nanoparticles modified g-C_3N_4 heterojunction photocatalyst: Influencing factors, products and mechanism insight. *Chin. Chem. Lett.* **2021**, *33*, 1337−1342.
(77) Wu, S.; Hu, H.; Lin, Y.; Zhang, J.; Hu, Y. H. Visible light photocatalytic degradation of tetracycline over TiO_2. *Chem. Eng. J.* **2020**, *382*, 122842.
(78) Wu, S.; Li, X.; Tian, Y.; Lin, Y.; Hu, Y. H. Excellent photocatalytic degradation of tetracycline over black anatase-TiO_2 under visible light. *Chem. Eng. J.* **2021**, *406*, 126747.
(79) Lv, C.; Lan, X.; Wang, L.; Dai, X.; Zhang, M.; Cui, J.; Yuan, S.; Wang, S.; Shi, J. Rapidly and highly efficient degradation of tetracycline hydrochloride in wastewater by 3D IO-TiO_2-CdS nanocomposite under visible light. *Environ. Technol.* **2021**, *42*, 377−387.
(80) Rani, S.; Garg, A.; Singh, N. Efficient degradation of doxycycline and ofloxacin in an aqueous environment using Fe and Cu doped TiO_2-SiO_2 photocatalyst under sunlight. *Environ. Eng. Res.* **2022**, *27*, 195−207.
(81) Wu, S.; Hu, H.; Lin, Y.; Zhang, J.; Hu, Y. H. Visible light photocatalytic degradation of tetracycline over TiO_2. *Chem. Eng. J.* **2020**, *382*, 122842.
(82) Kakavandi, B.; Bahari, N.; Rezaei Kalantary, R. R.; Dehghani Fard, E. D. Enhanced sono-photocatalysis of tetracycline antibiotic using TiO2 decorated on magnetic activated carbon (MAC@ T) coupled with US and UV: A new hybrid system. *Ultrason. Sonochem.* **2019**, *55*, 75−85.
(83) Rezaei, S. S.; Kakavandi, B.; Noorisepehr, M.; Isari, A. A.; Zabih, S.; Bashardoust, P. Photocatalytic oxidation of tetracycline by magnetic carbon-supported TiO_2 nanoparticles catalyzed peroxydisulfate: Performance, synergy and reaction mechanism studies. *Sep. Purif. Technol.* **2021**, *258*, 117936.
(84) Zhang, T.; Liu, Y.; Rao, Y.; Li, X.; Yuan, D.; Tang, S.; Zhao, Q. Enhanced photocatalytic activity of TiO_2 with acetylene black and persulfate for degradation of tetracycline hydrochloride under visible light. *Chem. Eng. J.* **2020**, *384*, 123350.
(85) Kubiak, A.; Bielan, Z.; Kubacka, M.; Gabała, E.; Zgoła-Grześkowiak, A.; Janczarek, M.; Zalas, M.; Zielińska-Jurek, A.; Siwińska-Ciesielczyk, K.; Jesionowski, T. Microwave-assisted synthesis of a TiO_2-CuO heterojunction with enhanced photocatalytic activity against tetracycline. *Appl. Surf. Sci.* **2020**, *520*, 146344.
(86) Mengting, Z.; Kurniawan, T. A.; Avtar, R.; Othman, M. H. D.; Ouyang, T.; Yujia, H.; Xueting, Z.; Setiadi, T.; Iswanto, I. Applicability of TiO_2 (B) nanosheets@ hydrochar composites for adsorption of tetracycline (TC) from contaminated water. *J. Hazard. Mater.* **2021**, *405*, 123999.
(87) Shi, Y.; Yang, Z.; Wang, B.; An, H.; Chen, Z.; Cui, H. Adsorption and photocatalytic degradation of tetracycline hydrochloride using a palygorskite-supported Cu_2O−TiO_2 composite. *Appl. Clay Sci.* **2016**, *119*, 311−320.
(88) Shi, Y.; Yan, Z.; Xu, Y.; Tian, T.; Zhang, J.; Pang, J.; Peng, X.; Zhang, Q.; Shao, M.; Tan, W.; Li, H.; Xiong, Q. Visible-light-driven AgBr−TiO_2-Palygorskite photocatalyst with excellent photocatalytic activity for tetracycline hydrochloride. *J. Clean. Prod.* **2020**, *277*, 124021.
(89) Naqvi, F. K.; Faraz, M.; Beg, S.; Khare, N. Synthesis and phase transformation studies of dysprosium-doped $Bi_4V_2O_{11}$ nanoparticles and their application in visible light photocatalytic degradation of tetracycline drug. *ACS Omega* **2018**, *3*, 11300−11306.
(90) Yan, M.; Wu, Y.; Liu, X. J. Photocatalytic nanocomposite membranes for high-efficiency degradation of tetracycline under visible light: An imitated core-shell Au-TiO_2-based design. *J. Alloys Compd.* **2021**, *855*, 157548.
(91) Chen, R.; Wang, X.; Zhu, L. Adsorption and Photocatalytic Degradation of Tetracycline by Porous g-C3N4/TiO2, **2022**, DOI: 10.21203/rs.3.rs-1172368/v1.
(92) Wang, W.; Han, Q.; Zhu, Z.; Zhang, L.; Zhong, S.; Liu, B. Enhanced photocatalytic degradation performance of organic contaminants by heterojunction photocatalyst $BiVO_4$/TiO_2/RGO and its compatibility on four different tetracycline antibiotics. *Adv. Powder Technol.* **2019**, *30*, 1882−1896.
(93) Xia, B.; Deng, F.; Zhang, S.; Hua, L.; Luo, X.; Ao, M. Design and synthesis of robust Z-scheme ZnS-SnS_2 nn heterojunctions for highly efficient degradation of pharmaceutical pollutants: Performance, valence/conduction band offset photocatalytic mechanisms and toxicity evaluation. *J. Hazard. Mater.* **2020**, *392*, 122345.
(94) Yan, X.; Ji, Q.; Wang, C.; Xu, J.; Wang, L. In situ construction bismuth oxycarbonate/bismuth oxybromide Z-scheme heterojunction for efficient photocatalytic removal of tetracycline and ciprofloxacin. *J. Colloid Interface Sci.* **2021**, *587*, 820−830.
(95) Lai, C.; Xu, F.; Zhang, M.; Li, B.; Liu, S.; Yi, H.; Li, L.; Qin, L.; Liu, X.; Fu, Y.; An, N.; Yang, H.; Huo, X.; Yang, X.; Yan, H. Facile synthesis of CeO_2/carbonate doped $Bi_2O_2CO_3$ Z-scheme heterojunction for improved visible-light photocatalytic performance: Photodegradation of tetracycline and photocatalytic mechanism. *J. Colloid Interface Sci.* **2021**, *588*, 283−294.
(96) He, X.; Kai, T.; Ding, P. Heterojunction photocatalysts for degradation of the tetracycline antibiotic: a review. *Environ. Chem. Lett.* **2021**, *19*, 4563−4601.
(97) Yang, Y.; Zeng, Z.; Zhang, C.; Huang, D.; Zeng, G.; Xiao, R.; Lai, C.; Zhou, C.; Guo, H.; Xue, W.; Cheng, M.; Wang, W.; Wang, J. Construction of iodine vacancy-rich BiOI/Ag@ AgI Z-scheme heterojunction photocatalysts for visible-light-driven tetracycline degradation: transformation pathways and mechanism insight. *Chem. Eng. J.* **2018**, *349*, 808−821.
(98) Yang, R.; Zhu, Z.; Hu, C.; Zhong, S.; Zhang, L.; Liu, B.; Wang, W. One-step preparation (3D/2D/2D) $BiVO_4$/$FeVO_4$@ rGO heterojunction composite photocatalyst for the removal of tetracycline and hexavalent chromium ions in water. *Chem. Eng. J.* **2020**, *390*, 124522.
(99) Tung, M. H. T.; Cam, N. T. D.; Van Thuan, D.; Van Quan, P.; Van Hoang, C.; Phuong, T. T. T.; Lam, N. T.; Tam, T. T.; Le Chi, N. T. P.; Lan, N. T. Novel direct Z-scheme AgI/N−TiO_2 photocatalyst for

https://doi.org/10.1021/acsomega.2c04576
ACS Omega 2022, 7, 33572−33586

removal of polluted tetracycline under visible irradiation. *Ceram. Int.* **2020**, *46*, 6012−6021.
(100) Chen, J.; Zhang, X.; Bi, F.; Zhang, X.; Yang, Y.; Wang, Y. A facile synthesis for uniform tablet-like TiO_2/C derived from Materials of Institut Lavoisier-125 (Ti)(MIL-125 (Ti)) and their enhanced visible light-driven photodegradation of tetracycline. *J. Colloid Interface Sci.* **2020**, *571*, 275−284.
(101) Salmanzadeh-Jamadi, Z.; Habibi-Yangjeh, A.; Pouran, S. R.; Xu, X.; Wang, C. Facile fabrication of TiO_2/Bi_5O_7Br photocatalysts for visible-light-assisted removal of tetracycline and dye wastewaters. *J. Phys. D: Appl. Phys.* **2022**, *55*, 165105.
(102) Oseghe, E. O.; Ofomaja, A. E. Facile microwave synthesis of pine cone derived C-doped TiO_2 for the photodegradation of tetracycline hydrochloride under visible-LED light. *J. Environ. Manage.* **2018**, *223*, 860−867.
(103) Darvishi, S.; Javanbakht, S.; Heydari, A.; Kazeminava, F.; Gholizadeh, P.; Mahdipour, M.; Shaabani, A. Ultrasound-assisted synthesis of MIL-88 (Fe) coordinated to carboxymethyl cellulose fibers: A safe carrier for highly sustained release of tetracycline. *Int. J. Biol. Macromol.* **2021**, *181*, 937−944.
(104) Bettany, J.; Wolowacz, R. Tetracycline derivatives induce apoptosis selectively in cultured monocytes and macrophages but not in mesenchymal cells. *Adv. Dent. Res.* **1998**, *12*, 136−143.
(105) Babín, M.; Boleas, S.; Tarazona, J. V. In vitro toxicity of antimicrobials on RTG-2 and RTL-W1 fish cell lines. *Environ. Toxicol. Pharmacol.* **2005**, *20*, 125−134.
(106) Bacon, J.; Linseman, D.; Raczniak, T. In vitro cytotoxicity of tetracyclines and aminoglycosides in LLC-PK1, MDCK and Chang continuous cell lines. *Toxicol. In Vitro* **1990**, *4*, 384−388.
(107) Chelimuge, Q.; Xiaoyu, Y.; Jiawei, L.; Wenjing, D.; Hao, C.; Huan, W.; Wenqing, C.; Jingfeng, Y.; Jianhua, Y.; Wu, D. Parental Tetracycline Hydrochloride Exposure and Resultant Offspring Cartilage Toxicity. *Asian J. Ecotoxicol.* **2021**, 235−244.
(108) Reeves, P. J.; Kim, J.-M.; Khorana, H. G. Structure and function in rhodopsin: a tetracycline-inducible system in stable mammalian cell lines for high-level expression of opsin mutants. *Proc. Natl. Acad. Sci.* **2002**, *99*, 13413−13418.
(109) Shockett, P.; Difilippantonio, M.; Hellman, N.; Schatz, D. G. A modified tetracycline-regulated system provides autoregulatory, inducible gene expression in cultured cells and transgenic mice. *Proc. Natl. Acad. Sci.* **1995**, *92*, 6522−6526.
(110) Izumi, M.; Gilbert, D. M. Homogeneous tetracycline-regulatable gene expression in mammalian fibroblasts. *J. Cell. Biochem.* **2000**, *76*, 280−289.
(111) Javvaji, K.; Begum, G.; Deshpande, S. S.; Rana, R. K.; Misra, S. Potential of the bioinspired $CaCO_3$ microspheres loaded with tetracycline in inducing differential cytotoxic effects toward non-cancerous and cancer cells: a cytogenetic toxicity assessment using CHO cells in vitro. *Chem. Res. Toxicol.* **2018**, *31*, 629−636.
(112) Kamali, A.; Mirlohi, M.; Etebari, M.; Sepahi, S. Occurrence of Tetracycline Residue in Table Eggs and Genotoxic Effects of Raw and Heated Contaminated Egg Yolks on Hepatic Cells. *Iran. J. Public Health* **2020**, *49*, 1355.
(113) Scaria, J.; Anupama, K.; Nidheesh, P. Tetracyclines in the environment: An overview on the occurrence, fate, toxicity, detection, removal methods, and sludge management. *Sci. Total Environ.* **2021**, *771*, 145291.
(114) Andriani, Y.; Ramli, N. M.; Syamsumir, D. F.; Kassim, M. N. I.; Jaafar, J.; Aziz, N. A.; Marlina, L.; Musa, N. S.; Mohamad, H. Phytochemical analysis, antioxidant, antibacterial and cytotoxicity properties of keys and cores part of Pandanus tectorius fruits. *Arabian J. Chem.* **2019**, *12*, 3555−3564.
(115) (a) Itoh, K.; Shigemi, H.; Chihara, K.; Sada, K.; Yamauchi, T.; Iwasaki, H. Caspofungin suppresses zymosan-induced cytokine and chemokine release in THP-1 cells: possible involvement of the spleen tyrosine kinase pathway. *Transl. Res.* **2021**, *227*, 53−63. European Centre for Disease Prevention and Control, European Centre for Disease Prevention and Control, an agency of the European Union (https://www.ecdc.europa.eu/en/antimicrobial-consumption/database/rates-country) (accessed Jan 20, 2022).

https://doi.org/10.1021/acsomega.2c04576
ACS Omega 2022, 7, 33572−33586